

Limitations of traditional models for perfusion

Constantin Sandmann, Erik A. Hanson, Alexander Malyshev, Arvid Lundervold, Jan Modersitzki, Erlend Hodneland

Abstract—Objective: In perfusion imaging the usage of traditional one-compartment models to estimate hemodynamic parameters like perfusion, blood volume and mean transit times is widespread. In this paper we set up a mathematical framework, clearly revealing the traditional models’ limitations related to perfusion recovery. **Methods:** We derive theoretical details for voxelwise perfusion estimation when the image resolution reaches the spatial scale of the capillary systems. Furthermore we analyse the transitional understanding of perfusion estimation using a continuous model for microcirculation and propagation of a tracer in the capillary tissue, understood as tissue perfused by capillaries. The effects are illustrated using porous media flow simulations. **Results:** Traditional one-compartment models only are equivalent to a continuous model for tracer transport when upstream effects can be counted for. This is however difficult to incorporate into practical applications. It is demonstrated that traditional models are accurately recovering perfusion if applied to the entire domain, but are not meaningful if applied to smaller portions of the system and will result in over estimation of perfusion. Evidence of real patient data is provided, indicating that this effect might also be observed on coarse scale in real-life applications. **Conclusion:** We find that traditional models for perfusion overestimate blood flow if applied to only parts of a coupled system. Estimation of the blood volume is stable and can also be applied in coupled systems. **Significance:** Awareness should be drawn to potentially inaccurate perfusion estimates in clinical applications. For the task of future perfusion estimations we suggest that continuous and coupled PDE models are developed.

I. INTRODUCTION

Quantitative measurements of hemodynamic medical parameters based on tracer kinetic modeling are widespread both in research and in clinical practice [1], [2], [3]. In the present work, we focus on mathematical models to estimate blood perfusion (cerebral blood flow, CBF), blood volume (cerebral blood volume, CBV), and mean transit time (MTT) of the brain from dynamic image data using intravascular tracers.

While hardware limitations in medical imaging for decades have confined studies to only handle larger tissue regions or full organs, modern imaging technology and voxel based analysis give rise to aspirations about detailed perfusion maps with sub-millimeter precision. Examples of estimated parameter maps can be found in [2], [3]. We expect the development to continue and that imaging systems will reach a resolution where a single capillary system spans over several voxels. Quantitative perfusion maps, as well as other parameter maps arising from tracer kinetic modeling, can be combined with anatomical information and have proven to be of particular value in e.g. stroke studies or localization of trauma. Among the physiological parameters obtainable from tracer kinetic modeling, CBF has been found particularly difficult to describe reliably on a voxel-basis [4]. These limitations are caused by issues of the numerical implementation [4], but might

also depend on over-simplified dynamic models, which were originally designed to describe larger volumes of interest [5].

Most commonly perfusion can be understood as the delivery of arterial blood to the capillary system. There have been several approaches to clarify this concept in a continuous sense. In [6], dispersion of the arterial input function was simulated using Navier-Stokes equations. It was shown that neglecting to account for dispersion can have adverse impact on perfusion measurements. In [7], the problem of scale dependent continuous perfusion was discussed. Perfusion defined as flow entering a voxel will scale with voxel size, and this notion of perfusion is therefore inappropriate. More recently a two-compartment model was introduced as a precise definition of local perfusion [8]. However, evaluation of the proposed modeling is still pending.

In this work we focus on the validity of traditional perfusion models. We demonstrate that traditional models like deconvolution or the maximum slope model are able to recover the perfusion accurately if applied to the entire domain fed by the incoming flow. However, when applying the traditional models to isolated parts of the full system, we find that local perfusion in coupled systems is not straightforward to define. In order to cope with this issue, two useful definitions of voxel-wise perfusion are presented: A definition P_v describing the local inflow into a voxel, but otherwise not fulfilling the traditional concept of perfusion, and then a tailored definition of perfusion P_s for continuous models.

The concepts are illustrated by simulations of flow in a tissue patch with one inlet, one outlet, and a capillary system in between. A directional flow field for the patch is set up according to Darcy’s law from porous media flow [9]. Contrast agent propagation in this patch is simulated using standard transport equations. We show that the discretized 3D system can be equivalently described by a coupled set of multiple traditional one-compartment models, in line with the physical environment where each control volume is feeding its direct neighbors.

Our results show that traditional models tend to overestimate P_s and underestimate P_v if they are applied only to parts of the full system. Analytic results are given, which show that the recovered perfusion depends on all upstream flow and not only on the local value. We also show results indicating that overestimation of perfusion due to coupling might also be present in real data.

II. TRADITIONAL MODELS FOR PERFUSION

In this section we describe the convolution- and the maximum slope model, two widely used one-compartment pharmacokinetic models for measurements of CBF and CBV [2],

[3], [4]. For the remaining, they are referred to as *traditional* models.

Let Ω_i be an arbitrary control volume with one inlet and one outlet, and let $C(t)$ denote the average contrast agent (CA) concentration within Ω_i at timepoint t . The traditional models assume that the change of concentration at timepoint t can be described by the ordinary differential equation

$$C'(t) = P_a c_a(t) - P_v c_v(t), \quad C(0) = 0. \quad (1)$$

Here c_a, c_v are the plasma CA concentrations at the inlet and outlet of Ω_i and P_a, P_v are the corresponding flow values at these locations. In the following it is assumed that the plasma tracer concentration c_a at the inlet is known. In clinical practice this can be accounted for by measuring c_a in a feeding artery [10]. Since c_v is usually unknown, additional assumptions need to be made if one wants to reconstruct P_a from a given tissue curve C . The convolution model and the maximum slope (MS) model diverge in further assumptions.

A. The Convolution Model

For the deconvolution model, one approach is to assume there is an unknown probability distribution of transit times h through Ω_i , cf. [1]. This leads to

$$P_v c_v(t) = P_a (h * c_a)(t) := P_a \int_0^t c_a(s) h(t-s) ds. \quad (2)$$

Combining this with (1) yields $C'(t) = P_a c_a(t) - P_a (h * c_a)(t)$. Integrating this equation and using basic properties of the convolution one obtains the general solution

$$C(t) = (I * c_a)(t). \quad (3)$$

where the *impulse response function* I is defined as $I(t) := P_a(1 - \int_0^t h(s) ds)$. The task of identifying $I(t)$ given a tissue curve $C(t)$ and an arterial input function $c_a(t)$ is a deconvolution problem. If $I(t)$ is recovered, P_a can subsequently be estimated as $P_a = \max_t I(t)$. There are several methods to perform the deconvolution. A standard approach using Fourier-based algorithms is sensitive to the presence of noise [10]. Another class of deconvolution algorithms gaining increasing attention are based on Bayesian modeling [11]. However the numerical handling is still difficult since complex and error-prone numerical integration has to be performed [11]. A popular class among deconvolution algorithms is based on singular value decomposition (SVD) [10]. These algorithms have shown to be robust for a reasonable noise level. Also, they can be easily adapted to be robust against delays in tracer arrival using block-circular structures (bSVD cf. [12]). In order to identify the impulse response function $I(t)$ from applied data, we hence decided to use the bSVD model as proposed in [12].

B. The Maximum Slope Model

In the MS model it is assumed that when c_a has its maximum, only a negligible amount of CA is leaving the system [13]. For this time interval, (1) reduces to

$$C'(t) = P_a c_a(t), \quad C(0) = 0. \quad (4)$$

One can see that if c_a has a maximum, also C' must have a maximum since stationarity in P_a is assumed. Hence, it holds that

$$P_a = \frac{\max_t C'(t)}{\max_t c_a(t)}. \quad (5)$$

III. A SYNTHETIC MODEL FOR CAPILLARY FLOW

The validity of the traditional methods rely on a ROI with only one inlet and one outlet. In fact, this assumption may easily be violated when we locally describe CA propagation through a larger volume with a highly developed capillary system. For this type of model system we instead expect a set of coupled transport equations where each voxel can be regarded as an inlet for surrounding voxels.

Hence, in order to make a realistic synthetic model for capillary flow, we decided to describe the CA propagation as a spatially coupled transport process, i.e. using partial differential equations (PDE) for transport. This PDE model is used for validation of the traditional models.

A major difference between our coupled flow model and traditional tracer kinetic modeling is the normalization of the flow field. To avoid a discretization dependent flow field for the PDE model, we instead use vector valued surface fluid flux $\mathbf{q} = \mathbf{q}(x)$ with units $[\text{mm}^3/(\text{s mm}^2)]$ as the fluid carrying quantity, in agreement with geoscience and porous media simulation theory. The fluid flux is a vector field describing the volume of fluid per unit time flowing across a sliced unit area of the sample. A detailed outline of how the flow field was obtained can be found in Section III-E. Apart from the normalization with respect to surface, the assumptions of linearity and stationarity in the fluid flux are in complete agreement with standard pharmacokinetic modeling [1].

A. A Model for Indicator Dilution

This section describes a model for CA propagation in the tissue as it is homogeneously dissolved in the evolving fluid. We assume that the CA is entering the domain along with the fluid flowing in via the source, and similarly extracted at a sink.

In order to define meaningful and continuous contrast agent concentrations, we first describe CA concentration in an (arbitrarily) small tissue volume $\Omega_\varepsilon(x)$. Let $V_\varepsilon(x)$ be the volume of an arbitrarily small control region and let $v_\varepsilon(x)$ be the blood volume within the same control region. Letting the control region go towards zero volume, the porosity $\phi(x) := v_\varepsilon(x)/V_\varepsilon(x)$ reflects the local space of the vascular system. The simplification of porosity as a continuous quantity is frequently performed in flow simulations. The flux $\mathbf{q}(x)$ $[\text{mm}^3/(\text{s mm}^2)]$ as well as the porosity $\phi(x)$ $[\text{mm}^3/\text{mm}^3]$ are assumed to be stationary and hence independent of time. We further introduce $C = C(x, t)$ and $c = c(x, t)$ as the CA concentration with respect to $V(x)$ and $v(x)$ respectively. By definition, we obtain the relation $C(x, t) = \phi(x)c(x, t)$. The rate of change of tracer molecules within a control volume Ω_i can hence be phrased as

$$\frac{d}{dt} \int_{\Omega_i} C dx = \int_{\Omega_i} \frac{d}{dt} (\phi c) dx = \int_{\Omega_i} \phi \frac{dc}{dt} dx, \quad (6)$$

where the assumption of stationary $\phi(x)$ was used. Since we expect mainly transport and marginal diffusion, the change in tracer mass within Ω_i occurs from advective flow and the source and sink field $Q(x)$. Let us write the source- and the sink term as $Q(x) = Q_{\text{si}}(x) + Q_{\text{so}}(x)$ where $Q_{\text{si}}(x) < 0$ is the sink and $Q_{\text{so}}(x) > 0$ is the source, and zero elsewhere. Note that $\int_{\Omega} Q dx = 0$. The change in contrast agent at time point t from fluid entering the control volume can be written as

$$-\int_{\partial\Omega_i} c(\mathbf{q} \cdot \mathbf{n}) ds + \int_{\Omega_i} c_a Q_{\text{so}} dx + \int_{\Omega_i} c Q_{\text{si}} dx, \quad (7)$$

where $\mathbf{n}(x)$ is the outward unit normal on $\partial\Omega_i$. In standard pharmacokinetic modeling, $c_a = c_a(x, t)$ is referred to as the arterial input function (AIF). From the principle of conservation of tracer molecules, (6) and (7) must balance for each control volume Ω_i , such that

$$\int_{\Omega_i} \phi \frac{dc}{dt} dx + \int_{\partial\Omega_i} c(\mathbf{q} \cdot \mathbf{n}) ds = \int_{\Omega_i} c_a Q_{\text{so}} dx + \int_{\Omega_i} c Q_{\text{si}} dx. \quad (8)$$

Equation (8) is consistent with the continuity equation on local form

$$\begin{cases} \phi \frac{\partial c}{\partial t} + \nabla \cdot (c\mathbf{q}) = c_a Q_{\text{so}} + c Q_{\text{si}} & x \in \Omega, t > 0, \\ c(x, t) = 0 & x \in \Omega, t = 0. \end{cases} \quad (9)$$

where we also added the initial condition $c(x, 0) = 0$ in line with the physical problem of no tracer at $t = 0$. Equation (9) is a linear transport equation in $c(x, t)$. Following [14], (9) admits a unique local solution.

B. Relating the transport equation model with the traditional deconvolution model for perfusion

In this section we describe how the continuous model is related to the traditional deconvolution model. More specifically, we will show that in the continuous model, the flow into each voxel can be described by a traditional model with arterial input determined by adjacent upstream voxels.

Let us start by modeling the CA concentration in a given voxel Ω_i using traditional models. For sake of simplicity we assume that $Q_{\text{so}} = Q_{\text{si}} = 0$ within that voxel. Note that it is possible to extend the following approach also to voxels where this is not the case. Define the outward normal vector \mathbf{n} and areas (voxel faces) of inflow and outflow over the boundary as $S_{\text{in}} := \{x \in \partial\Omega_i : \mathbf{q} \cdot \mathbf{n} < 0\}$ and $S_{\text{out}} := \{x \in \partial\Omega_i : \mathbf{q} \cdot \mathbf{n} > 0\}$ respectively. For the domain Ω_i we define the arterial input c_{in} as the weighted average of the tracer flux across S_{in}

$$c_{\text{in}}(t) := \frac{\int_{S_{\text{in}}} (\mathbf{q} \cdot \mathbf{n}) c ds}{\int_{S_{\text{in}}} \mathbf{q} \cdot \mathbf{n} ds}. \quad (10)$$

This allows us to define the perfusion P_v within Ω_i as the total fluid inflow divided by the volume,

$$P_v := -\frac{1}{\text{Vol}(\Omega_i)} \int_{S_{\text{in}}} \mathbf{q} \cdot \mathbf{n} ds. \quad (11)$$

Given an incompressible flow, let us now assume that the rate of fluid entering the region is the same as the rate

of fluid leaving it. Further let $c_i(t)$ denote the average CA concentration within Ω_i . Then it holds that $P_v = P_{\text{out}}$ and we can describe c_i by the traditional model (1),

$$(\phi c_i)'(t) = P_v(c_{\text{in}}(t) - c_{\text{out}}(t)). \quad (12)$$

Note that the upwind-discretization described in Section III-A models each voxel as a well-mixed compartment: it is assumed that the CA concentration at the outflow S_{out} equals the concentration within the voxel and that the concentration at the inflow is the concentration within the adjacent voxels.

In this case it follows that (12) reduces to $(\phi c_i)'(t) = P_v(c_{\text{in}}(t) - c_i(t))$ with solution

$$C_i(t) = \phi_i(J_i * c_{\text{in}})(t) \text{ for } J_i(t) = (P_v/\phi_i)e^{-(P_v/\phi_i)t}. \quad (13)$$

The arterial input c_{in} is determined by (10), which recursively depends on all upstream voxels until the global arterial input is reached. To verify this relationship numerically, we simulated a tissue curve $C_i(t)$ using both the continuous PDE model as well as recursive convolution by (13). We refer to the latter approach as *local convolution*. The two curves have an almost perfect match, as seen in Figure 1 (left).

As a direct consequence, it follows by recursion that the concentration at a voxel i can be written as a convolution of the (global) arterial input function with a weighted average of all upstream impulse response functions. Deconvolving a tissue concentration C_i with the global AIF will yield an impulse response function which depends not only on the local flow and porosity, but on flow and porosity of all upstream voxels. In the special case that transport is occurring only along one row of voxels, as e.g. in the top row of our synthetic example, the concentration in voxel i is given by

$$C_i(t) = \phi_i(J_1 * \dots * J_{i-1} * c_a)(t). \quad (14)$$

where $J_i(s) := p_i \exp(-p_i(s))$ for $p_i = P_v^i/\phi_i$. An analytic expression for the convolution of finitely many functions J_i can be found in [15]. This relationship was also confirmed experimentally: Figure 1 (right) shows the impulse response function determined by (14) and the numerically achieved impulse response function obtained from deconvolving a tissue curve of the continuous model with the global arterial input function. The simulation was performed at location (1,20) of the software phantom. The two curves coincide almost perfectly, highlighting the validity of the established theory.

These results show that the PDE model and the convolution model are equal in terms of local, voxelwise flow estimates if the convolution model is applied with the correct, local arterial input. Also, the impulse response function obtained by convolution of the global arterial input function is identical to an analytical recursive convolution along all upstream voxels. This clearly demonstrates that the perfusion which is recovered by traditional models will depend on all upstream flow. However, for meaningful results the entire streamline length within the capillary system needs to be taken into consideration, where the blood is providing the tissue with nutrients and oxygen.

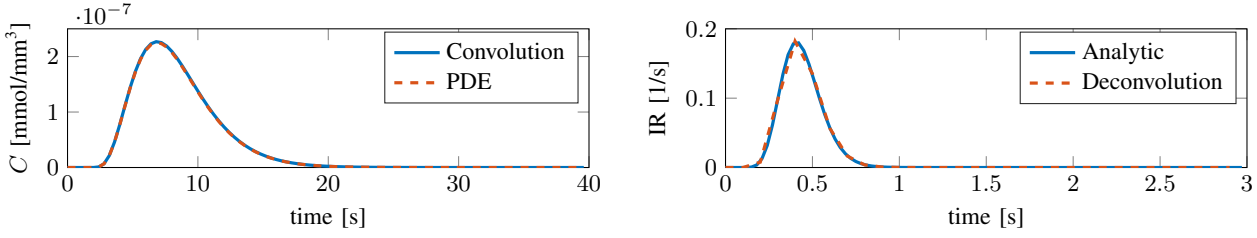


Figure 1. Left: Red curve shows the tissue concentrations (C) of the continuous PDE model at location [32,35]. Blue curve shows recursive convolution by (13) with experimental values of $P_v^i = 5328 \text{ ml/min/100ml}$ and c_{in} taken locally from upstream voxels around the simulated voxel. The two curves have an almost perfect overlap. Note that the numbers used for the perfusion is unrealistically high since normalization is performed with respect to the volume of only one voxel. Right: Red curve shows the computed impulse response functions (IR) at location [1,20] using the global arterial input function. Blue curve shows the analytic impulse response function given by (14). The two curves have an almost perfect overlap. These numerical experiments support the analytic considerations, that the computed impulse response function by traditional methods is not the directly feeding impulse response function, but rather a recursive impulse response function depending on all upstream voxels.

C. Relating Flow with Perfusion

The model described in (26) uniquely determines the flux field $\mathbf{q}(x)$. However, in pharmacokinetic modeling the parameter of interest is usually CBF, which we will denote by $P(x)$ as the voxelwise field of perfusion. The surface flux and perfusion are physically distinct, and there are at least two differences between $\mathbf{q}(x)$ and $P(x)$. First, the flux is a vector field and the perfusion is a scalar field. Second, the flux is normalized to a surface area and the perfusion is normalized to a volume. Hence the flux describes flow and transport over a surface separating spatial regions, while the perfusion describes blood leaving/entering a compartment within a given volume.

More specifically, the common understanding of perfusion $P(x)$ is the amount of blood feeding a tissue volume per unit time, with units $[\text{mm}^3/(\text{s mm}^3)]$. In this work we address the fine scale setting, where the perfusion is taking place on voxel level. At this level, a clearer understanding of how perfusion relates to flows and fluxes is desirable.

One straightforward approach for converting flux into perfusion could be to estimate the perfusion as the total inflow (or outflow) of fluid (e.g. arterial blood) into a control region per unit time, and then normalizing with the control region volume. This is a valid approach only if the control regions are not feeding each other, and is therefore well-founded for the entire organ, in line with the theoretical foundation of traditional compartment models for perfusion where a control region has its own source of feeding arterial blood, independent of neighbour regions.

If the control region is a single voxel or a sub-division of a capillary system with sequentially feeding arterial blood, the traditional model assumptions are violated since every control region will feed its neighbours, thus becoming a coupled system of flow. Simply summing the total inflow into a voxel and dividing by the voxel volume will strongly over-estimate the perfusion as the normalization refers to the wrong volume. This phenomenon is demonstrated in Figure 2 where the volume on the left has the true perfusion of $P_1 = F_0/(2V)$ for an incoming flow F_0 $[\text{mm}^3/\text{s}]$ and distribution volume $2V$ $[\text{mm}^3]$. However, for another discretization as shown in the middle, the perfusion within each of these sub-volumes becomes $P_2 = F_0/V = 2P_1$. Taking the average across the two sub-volumes, it is clear that the perfusion is over-estimated with a factor of two. A discretization dependent perfusion

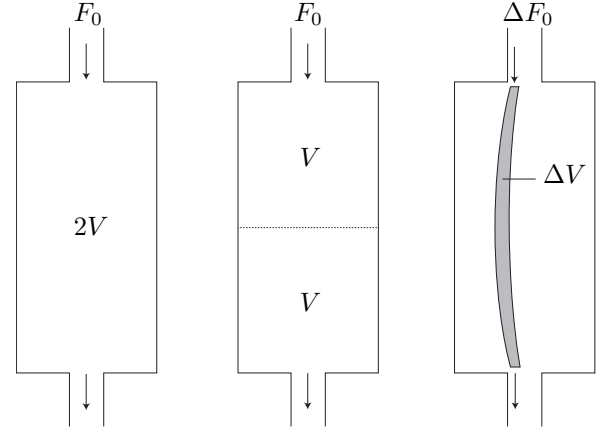


Figure 2. Perfusion within a small volume. Left: A compartment with volume $2V$ is exposed to a flow F_0 $[\text{mm}^3/\text{s}]$ of fluid. By definition, the perfusion within this compartment becomes $P_1 = F_0/(2V)$. Middle: The same volume is divided into two compartments (e.g. voxels), and the perfusion for each of the compartments becomes $P_2 = F_0/V = 2P_1$. The discrepancy between the two discretizations occurs because the flow is counted twice as it is fed from one voxel to the other. Right: As a solution to the described problem we rather pick out a true distribution volume ΔV (area in this 2D sketch), which is a small area around a given streamline along the centre line of the grey area. This is the true distribution volume (area in this 2D sketch) which is fed with arterial blood from the incoming fractional flow ΔF_0 . The correct perfusion within ΔV is therefore $\Delta F_0/\Delta V$. The entire compartment can further be divided into similar infinitesimal distribution volumes, thus providing locally correct perfusion estimates.

estimate is not recommendable, and the perfusion estimate of P_2 is clearly wrong. This problematic issue was already identified by [7], stating that an incorrect normalization will lead to multiple counting of the same flow, and hence an over-estimation of perfusion.

In the following we introduce a meaningful notion of perfusion for the fine scale continuous model. To do this, we will consider distribution volumes which are following the streamlines, as shown in Fig. 2 (right). For each point of a streamline we will select a small perpendicular disk with radius chosen in such a way that the total flow over each disk is constant along the streamline.

More precisely, let us consider an arbitrary streamline $S \subseteq \Omega \subseteq \mathbb{R}^3$ of length $l > 0$ and parametrization $s : [0, l] \rightarrow S$. We start by calculating the total flow over a small 2-D disc perpendicular to the streamline. Let $y \in S$ be an arbitrary location along the streamline. The total flow F over a 2-D

disc $B(y, R(y))$ perpendicular to the flow field $\mathbf{q}(y)$, centered at y and with radius $R : S \rightarrow \mathbb{R}^+$, is given by

$$F(y, R(y)) = \int_{B(y, R(y))} \mathbf{q}(x) \cdot \nu \, dx \text{ where } \nu := \mathbf{q}(y)/|\mathbf{q}(y)|. \quad (15)$$

In order to calculate the perfusion, we need to establish the volume of a small tube around the streamline. We will not consider a tube with constant radius, but one with spatially varying radii $r : [0, l] \rightarrow \mathbb{R}^+$. The total volume of such a tube surrounding the streamline is given by

$$V(r) = \int_0^l r(u)^2 \pi \, du. \quad (16)$$

Note that $R(y) := r(u)$ for some $u \in [0, l]$ satisfying $y = s(u)$. We define the perfusion at the arbitrary point y on the streamline as

$$P_s(y) := \lim_{\varepsilon \rightarrow 0} \frac{F(y, \varepsilon R(y))}{V(\varepsilon r)} \text{ for } R(y) := 1/\sqrt{|\mathbf{q}(y)|}. \quad (17)$$

In this expression the radii $R(y)$ are chosen in such a way that in the limit when $\varepsilon \rightarrow 0$, the perfusion is constant along the streamline. To see this, let us assume that \mathbf{q} is differentiable with Jacobian J . Using a Taylor expansion of $\mathbf{q}(x)$ around y , the Lagrange remainder theorem, as well as a change of coordinates $z = (x - y)/(\varepsilon R)$ yields

$$F(y, \varepsilon R(y)) = \varepsilon^2 \left(\pi + \varepsilon \int_{B(0,1)} \nu^\top J(\zeta) z R(y)^3 \, dz \right) \quad (18)$$

where $\zeta \in (0, z)$ and simplifications are due to $R(y) = 1/\sqrt{|\mathbf{q}(y)|}$ and $\nu := \mathbf{q}(y)/|\mathbf{q}(y)|$. Combining this result with (17) yields

$$P_s(y) = \left(\int_0^l r(u)^2 \, du \right)^{-1}. \quad (19)$$

Note that Equation (19) is independent of the spatial location y along the streamline and an explicit formula for converting flux into perfusion, showing that the perfusion scales with the streamline length l , as well as with the geometry of the domain, represented by the radii $r(u)$.

D. A Method to Estimate local Porosity

Porosity and CBV have the same definition, and we can therefore state that $\phi \equiv CBV$. It is known from literature on traditional models [1] for perfusion that CBV for the entire compartment can be expressed as

$$\phi = \frac{\int_0^\infty C \, dt}{\int_0^\infty c_a \, dt}. \quad (20)$$

where $C(t)$ is the tracer concentration with respect to a well mixed compartment and $c_a(t)$ is the tracer plasma concentration of the arterial input. However, it is not obvious that (20) is valid also for a continuous one-compartment field model where the voxels are feeding each other. We will now show that (20) is nevertheless valid.

Returning to the local definition of fluid tracer concentration $c(x, t)$, outside the source and sink area where $Q(x) = 0$ the PDE (9) is consistent with

$$\phi \frac{\partial c}{\partial t} = -\mathbf{q} \cdot \nabla c. \quad (21)$$

Integrating, using the boundary conditions $c(x, 0) = c(x, \infty) = 0$ and defining $E(x) := \int_0^\infty c(x, t) \, dt$ leads to

$$0 = \mathbf{q} \cdot \nabla E(x). \quad (22)$$

We can interpret this equation such that \mathbf{q} is tangent to the level-sets of the function $E(x)$, which means that $E(x)$ is constant along the streamlines of the fluid flow. Since at the beginning of the streamline it holds by construction that $c(x_0, t) = c_a(t)$ and since $C(x, t) = \phi(x)c(x, t)$ the claim (20) follows when we pick out E for the arterial input function and for any other point on the streamline.

E. Simulations of capillary flow

In this section we will describe how we construct the vector flow field $\mathbf{q}(x)$ which drives the transport. This modeling is in agreement with the assumption of stationary, incompressible flow at low Reynold numbers within the capillary system [16] and with previous work on capillary perfusion simulations [17], [18].

For the time being we will not consider contrast agent concentrations, but only the fluid flow in general. The fluid density is denoted by $\rho = \rho(x, t)$ [mg/mm³]. Fluid entering and leaving the system is described by a source- and sink term $\tilde{Q} = \tilde{Q}(x)$ [mg/(s mm³)]. The continuity equation assuring conservation of fluid mass states

$$\frac{\partial(\phi\rho)}{\partial t} + \nabla \cdot (\rho\mathbf{q}) = \tilde{Q}. \quad (23)$$

Furthermore, assuming that the fluid flow is steady-state and that the density of blood ρ is constant in space, we obtain $\nabla \cdot \mathbf{q} = \tilde{Q}/\rho$. In order to scale away the density ρ , define Q [mm³/(s mm³)] having the relation $\tilde{Q} := Q\rho$, thus transforming (23) into

$$\nabla \cdot \mathbf{q} = Q. \quad (24)$$

Here the right hand side is a volume flux, only non-zero within the source or the sink. Elsewhere, (24) is concurrent with divergence free flow of an incompressible fluid. Low velocity fluid flux in porous media is usually described by Darcy's law. Neglecting gravitational forces [9] leads to:

$$\mathbf{q} = -\frac{\mathbf{k}}{\mu} \nabla p. \quad (25)$$

Here, $\mathbf{k} = \mathbf{k}(x)$ is the intrinsic permeability tensor, $p = p(x)$ is the pressure, and $\mu = \mu(x)$ is the viscosity of the fluid. For simplicity, we will assume that \mathbf{k} is a symmetric and positive definite tensor with only nonzero diagonal elements $k_{ii} = k$, in accordance with a homogeneous porous medium. Equations (24) and (25) can be combined, yielding the following elliptic partial differential equation in the pressure field p within the closed domain Ω ,

$$\left| \begin{array}{ll} \nabla \cdot \left(-\frac{\mathbf{k}}{\mu} \nabla p \right) = Q, & x \in \Omega \\ n \cdot \nabla p = 0, & x \in \partial\Omega. \end{array} \right| \quad (26)$$

For the outward unit normal $n = n(x)$, Neuman boundary conditions are reflecting zero fluid flux $\mathbf{q}(x)$ across the boundary $\partial\Omega$. After solving (26) for the pressure p , the flux field can be estimated according to (25) from the obtained pressure map.

F. Numerical Implementation

Using (26) and (9) we set up a forward simulation of blood flow and indicator dilution through the capillary system. We aimed at creating a generic synthetic test case and kept all optional parameters as simple as possible.

A standard arterial input function was chosen [10], the gamma-variate function $c_a(t) := D_0(t - t_0)^\alpha e^{-(t-t_0)/\beta}$ for default parameters $\alpha = 3$, $D_0 = 1 \text{ mmol}/(1\text{s})$, $\beta = 1.5\text{s}$ and $t_0 = 0\text{s}$. Ground truth perfusion was chosen as $50 \text{ ml}/\text{min}/100\text{ml}$, within the average range reported for human brain perfusion [19], [20]. The field of view was chosen as $3 \text{ mm} \times 3 \text{ mm} \times 1 \text{ mm}$, within the same order as the characteristic length of the capillary bed or individual capillaries, ranging from 0.1 mm to 3 mm [16], or 0.25 mm to 850 mm [21]. The source term was assigned to the upper left voxel and the sink term was assigned to the lower right voxel. The source can be understood as the arterial compartment, the sink as the venous compartment, and the remaining field of view as the capillary system. Permeability was chosen to be isotropic and constant throughout the domain $\mathbf{k} = k\mathbf{I}$ for the identity \mathbf{I} and $k = 5 \times 10^{-6} \text{ mm}^2$. Dynamic blood viscosity was chosen as $\mu = 5 \times 10^{-6} \text{ kPas}$ according to [22]. Porosity (e.g. CBV) was assumed to be $\phi = 0.05$, in line with measured CBV of the brain [20]. A voxel size of $0.05 \text{ mm} \times 0.05 \text{ mm} \times 1 \text{ mm}$ was applied for the PDE model, but later relaxed when reconstructing perfusion by the traditional methods. From the porous media model using (26) and (9), streamlines were found from tracking of the flux vector field \mathbf{q} by FACT [23], known from tractography within diffusion tensor imaging (DTI). The flow field obtained by the PDE model is visualized in Figure 3 (a).

Equation (26) was solved numerically using two-point flux-approximation (TPFA), well known within porous media simulations [24]. The transport of CA described in (8) was implemented using first order upwinding [25], yielding a discrete 2D+time CA concentration map $C(x_i, t_j)$.

G. Reconstruction of perfusion within synthetic data

We tested the convolution based traditional model (bSVD) (3) as well as maximum-slope (MS) model (5) for their capability to recover perfusion, and both models were compared to ground truth perfusion values. Prior to reconstruction, the CA concentration map $C(x_i, t_j)$ was downsampled to a time-resolution of 0.1 s . In order to simulate different spatial resolutions of the scanning process, the data was averaged using different block-sizes ranging from $(1, 1)$ pixel (i.e. same resolution as the PDE model) to $(64, 64)$ pixels (i.e. entire domain). Success of restoration was measured in terms of averaged relative error of the recovered perfusion with respect to the ground truth perfusion, $RE := (P_{\text{rec}} - P_{\text{true}})/P_{\text{true}} \cdot 100\%$. The recovered perfusion P_{rec} was compared against the two perfusion maps $P_{\text{true}} = \{P_v, P_s\}$ depicted in Figure 3.

The local perfusion map P_v was set up according to (11). Since normalization is performed with respect to voxel size, the values are unrealistically high and will vary with the discretization. As (13) shows, this can nevertheless be regarded a valid definition of perfusion since it models the feeding of arterial blood to a control region.

The global perfusion map P_s was set up using the definition along the streamlines (19). This definition most accurately reflects the physical perfusion at a given location and shows plausible perfusion values, cf. Figure 3. As an internal control, the average of P_v was found to be $49.59 \text{ ml}/\text{min}/100\text{ml}$, for all practical means identical to the global input perfusion of $50 \text{ ml}/\text{min}/100\text{ml}$. However, we do not expect the traditional models to be able to recover these values either. To quantify the errors occurring by traditional methods, the global arterial input function was used for the deconvolution, as measured in the source.

Results from deconvolution by traditional methods are displayed in Table I. For the complete domain (i.e. block size 64×64), both the MS method as well as the convolution method were able to restore the ground truth perfusion of $50 \text{ ml}/\text{min}/100\text{ml}$ accurately with errors of $< 1\%$ and $< 4\%$ respectively. However, the errors are increasing as methods are applied to smaller blocks of the system. If compared to P_v , one can see that results are improving with increasing block size. Note that the block size of $(0.5, 0.5)\text{mm}$ is within the range of resolution available on clinical scanners today, and is therefore clinically interesting. Also a clear advantage of the bSVD method as compared to MS can be observed for larger block sizes.

Results from reconstructing the porosity ϕ (i.e. CBV) according to (20) are also shown in Table I. The errors are low, independent of block size.

Table I
MEAN RELATIVE ERROR RE AND STANDARD DEVIATION (BOTH IN %) OF RECONSTRUCTED PERFUSION COMPARED TO THE GROUND TRUTH VALUES P_v , CBV, AND P_s FROM THE DIGITAL PHANTOM. BOTH RECONSTRUCTION MODELS MS AND bSVD ARE ABLE TO RESTORE THE PERFUSION FOR THE ENTIRE DOMAIN, BUT FAIL WHEN DIVIDING THE DOMAIN INTO SMALLER BLOCK SIZES. ON THE OTHER HAND, THE BLOOD VOLUME ϕ IS RECOVERED ACCURATELY, INDEPENDENT OF BLOCK SIZE. P_s IS ONLY DEFINED WITHIN A COUPLED SYSTEM HAVING STREAMLINES AND CAN THEREFORE NOT BE COMPARED WITH RESTORED PERFUSION FOR THE ENTIRE DOMAIN.

		block size (mm)			
		(0.05,0.05)	(0.23,0.23)	(0.47,0.47)	all
P_v	bSVD	-93%±4%	-67%±16%	-50%±23%	4%
	MS	-98%±2%	-88%±6%	-79%±11%	<1%
CBV	bSVD	<1%	<1%	<1%	<1%
	MS	<1%	<1%	<1%	<1%
P_s	bSVD	753% ± 926%	650% ± 757%	476% ± 507%	
	MS	124% ± 79%	114% ± 66%	103% ± 51%	

H. Reconstruction of perfusion within real data

Experimental results from Section III-G indicate that application of the deconvolution model to patches of tissues would lead to over estimation of blood flow as compared to the overall flow within the volume of interest. In order to illustrate that this effect also may be observed on a complete dataset, we applied the deconvolution model to

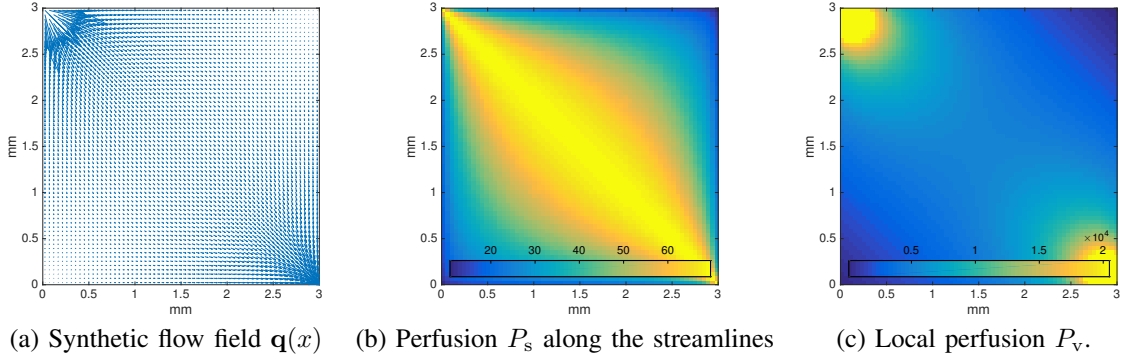


Figure 3. Porous media (PM) flow model with a source in the upper left corner and a sink in the lower right corner. (a) Flow field by the PDE model used to simulate distribution of the contrast agent. (b) Perfusion along the streamlines according to (19). (c) Local perfusion according to (11).

a clinically acquired human perfusion CT dataset of a 56 years old male male admitted with suspicion of stroke to the Radboud University Medical Center in Nijmegen, the Netherlands. The perfusion scan was obtained using a Toshiba Aquilon ONE scanner, pixel-size $0.43 \text{ mm} \times 0.43 \text{ mm}$, slice thickness 0.5 mm , contrast agent 50 ml Xentix 300, total scan-time 114 s , time resolution ranging from 2.1 s in the early- to 30 s in the late phase of CA uptake. The arterial input function was manually selected by a medical expert within the middle cerebral artery (MCA). Since we expected to see local over estimation effects mainly for small voxel sizes, the data was processed at full resolution ($512 \times 512 \times 320$) voxels. However, in order to deal with noise it was necessary to apply a prior gaussian smoothing with standard deviation of 1 voxel. Relative concentrations were estimated from the CT signal assuming a spatially independent proportionality constant. The brain tissue was segmented automatically and used as ROI for the perfusion analysis.

CBF was then estimated voxelwise using an own Matlab implementation of bSVD, yielding an average scaled CBF of $64.357 \text{ ml/min/100mg}$. Furthermore, we estimated the perfusion for the whole volume of interest by averaging the concentration values first and then performing the bSVD, yielding a total scaled CBF of $24.791 \text{ ml/min/100mg}$. Voxelwise results are depicted in Figure III-H.

IV. DISCUSSION

In this work we have studied the impact of traditional 1C models to perfusion reconstruction in a coupled system of blood flow in the capillary system. To establish ground truth values, we developed a PDE based digital phantom to simulate blood flow as porous media flow within a slab of capillary tissue. We have justified that the discretized PDE problem can be equivalently described as a system of coupled traditional one-compartment models.

Our results strongly support the usage of traditional models for entire regions which are exclusively fed by the measured arterial input. However, they also show that if traditional models are applied only to parts of the system, they tend to overestimate the actual perfusion. These limitations are only partly known to the community, and studies reporting voxel wise perfusion are continuously published [26], [27], [28]. Thus, a major motivation for our study is to stimulate the

awareness around this topic to push the development of more appropriate models. There are at least two issues related to the overestimation of perfusion. The first issue is that blood passing through a voxel without being locally delivered to the capillary tissue will contribute to artificially high perfusion values. The second issue is thoroughly studied in this work, and relates to estimation of the correct distribution volume used for computing the perfusion. As soon as there is dependency of capillary flow between adjacent voxels, the correct distribution volume used for normalizing the absolute flow into perfusion (i.e. ml/min/100ml) is not known and over-estimation of perfusion will occur. Using local arterial input functions is no remedy for this problem, since the resulting perfusion will depend heavily on the voxel size and overestimate the actual flow, cf. Figure 2 and (13).

The results from the digital phantom are supported by real data experiments, where we showed local overestimation of perfusion for small voxel-sizes as compared to an averaging of concentrations for the entire volume of interest. Regarding the CBV estimates, one can observe from Table I that estimation of blood volume is far more stable, and even various block sizes had little impact on the results. These results are in well agreement with the analytical considerations in Section III-D, stating that (20) is valid for entire organs as well as for single voxels. Thus, these results support the usage of (20) for computing the CBV with high accuracy for any type of block size, including single voxels.

Furthermore we have introduced two definitions of voxelwise perfusion. The perfusion P_s models perfusion along the streamlines and most accurately reflects the physical notion of volume flow within the correct distribution volume according to mathematical definitions. We showed that P_s is a global quantity along the streamline, and scales with streamline length and geometry. Theory and experiments show that the traditional models cannot recover this perfusion. The usage of P_s for reconstruction of perfusion in real data might as well be challenging as the entire geometry and microscopical flow patterns would have to be known to track the streamlines. However, for our purpose P_s was useful to clarify the concept of perfusion as a flow that must be normalized along its entire capillary length, when the blood undergoes a transition from arterial to venous blood. For future developments of field models, multi compartment models as suggested in [8] might

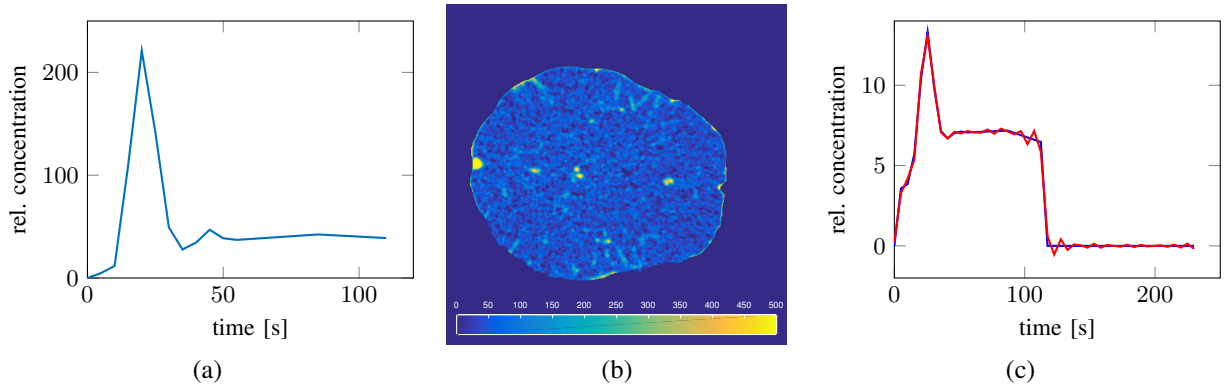


Figure 4. Results from real-data experiments (see Sec. III-H for details on the data). (a) AIF manually selected from the MCA. (b) One slice of the voxel-wise scaled CBF-reconstruction [ml/min/100mg] for a 3D volume of interest. (c) Mean concentration curve for the complete 3D volume of interest and the curve approximation by bSVD.

be more applicable, where the perfusion was suggested as the non-zero divergence of the arterial flux.

Perfusion P_v was set up based on the interpretation of a coupled system between adjacent voxels. Theory and examples show that this definition of perfusion does not comply with the physical understanding of perfusion since it depends heavily on the discretization. However, we have shown that traditional models would restore this local value if the local arterial input function was selected. We have additionally analyzed, both analytically and experimentally, the impact of selecting a further upstream arterial input function. Specifically, we have justified that traditional perfusion measurements based on convolution will identify the recursive impulse response function for all upstream voxels according to (14). Locally, the correct distribution volume is not accounted for and the obtained perfusion will be overestimated compared to the actual perfusion. The coupling between the continuous model and the convolution model in Section III-B demonstrates that the two approaches physically provide the same results, and there is no contradiction between them. The problematic issue of the traditional models is related to physical interpretation and normalization with respect to correct distribution volume.

V. CONCLUSION

In conclusion, our experiments show that if traditional methods for perfusion estimation are applied to a coupled system they perform well if applied to the entire domain, but tend to fail when applied to only parts of the system. We have illustrated this effect in detail in the case of high resolution images where the voxel size reaches the spatial dimension of the capillary systems, but also showed the effect on coarse scale real data. The reason for this failure is not numerical instabilities in the deconvolution, but rather that perfusion becomes overestimated since traditional models will not account for the correct distribution volume. This problem is expected to become more pronounced in future as imaging hardware is constantly improving in spatial resolution. We expect to find overestimation also in pathological tissue, where fluid is passing through multiple, adjacent voxels, and recommend to be take this effect into consideration in clinical evaluation of the data. To account for this problem, the development of new

field models for perfusion is therefore highly demanded, in line with approaches described in [8], [18].

REFERENCES

- [1] S. P. Sourbron and D. L. Buckley, "Classic models for dynamic contrast-enhanced MRI," *NMR Biomed*, vol. 26, no. 8, pp. 1004–1027, 2013.
- [2] Q. Feng *et al.*, "Voxel-level comparison of arterial spin-labeled perfusion magnetic resonance imaging in adolescents with internet gaming addiction," *Behav Brain Funct*, vol. 9, no. 1, p. 33, 2013.
- [3] Y. Chen *et al.*, "Voxel-level comparison of arterial spin-labeled perfusion MRI and FDG-PET in alzheimer disease," *Neurology*, vol. 77, no. 22, pp. 1977–1985, 2011.
- [4] K. Kudo *et al.*, "Differences in CT perfusion maps generated by different commercial software: Quantitative analysis by using identical source data of acute stroke patients 1," *Radiology*, vol. 254, no. 1, pp. 200–209, 2010.
- [5] K. L. Zierler, "Indicator dilution methods for measuring blood flow, volume, and other properties of biological systems: a brief history and memoir," *Ann Biomed Eng*, vol. 28, no. 8, pp. 836–848, 2000.
- [6] F. Calamante, P. Yim, and J. Cebal, "Estimation of bolus dispersion effects in perfusion MRI using image-based computational fluid dynamics," *Neuroimage*, vol. 19, no. 2, pp. 341–353, 2003.
- [7] R. M. Henkelman, "Does IVIM measure classical perfusion?" *Magn Reson Med*, vol. 16, no. 3, pp. 470–475, 1990.
- [8] S. P. Sourbron, "A tracer-kinetic field theory for medical imaging," *IEEE Trans Med Imaging*, 2014.
- [9] H. Darcy, "Les fontaines publiques de la ville de dijon," *Victor Dalmont*, p. 647, 1856.
- [10] L. Østergaard *et al.*, "High resolution measurement of cerebral blood flow using intravascular tracer bolus passages. part I: Mathematical approach and statistical analysis," *Magn Reson Med*, vol. 36, no. 5, pp. 715–725, 1996.
- [11] T. Boutelier *et al.*, "Bayesian hemodynamic parameter estimation by bolus tracking perfusion weighted imaging," *IEEE T Med Imaging*, vol. 31, no. 7, pp. 1381–1395, 2012.
- [12] O. Wu *et al.*, "Tracer arrival timing-insensitive technique for estimating flow in mr perfusion-weighted imaging using singular value decomposition with a block-circulant deconvolution matrix," *Magn Reson Med*, vol. 50, no. 1, pp. 164–174, 2003.
- [13] E. Klotz and M. König, "Perfusion measurements of the brain: using dynamic CT for the quantitative assessment of cerebral ischemia in acute stroke," *Eur J Radiol*, vol. 30, no. 3, pp. 170–184, 1999.
- [14] L. Evans, *Partial differential equations*, 2nd ed. Providence, Rhode Island: American Mathematical Society, 1998.
- [15] W. Kordecki, "Reliability bounds for multistage structures with independent components," *Stat Probabil Lett*, vol. 34, no. 1, pp. 43–51, 1997.
- [16] Y.-I. Cho and D. J. Cho, "Hemorheology and microvascular disorders," *Korean Circ J*, vol. 41, no. 6, pp. 287–295, 2011.
- [17] A. N. Cookson *et al.*, "A novel porous mechanical framework for modelling the interaction between coronary perfusion and myocardial mechanics," *J Biomech*, vol. 45, no. 5, pp. 850–855, 2012.

- [18] C. Michler *et al.*, "A computationally efficient framework for the simulation of cardiac perfusion using a multi-compartment Darcy porous-media flow model," *Int J Numer Method Biomed Eng*, vol. 29, no. 2, pp. 217–232, 2013.
- [19] W. D. Obrist *et al.*, "Cerebral blood flow and metabolism in comatose patients with acute head injury: relationship to intracranial hypertension," *J Neurosurg*, vol. 61, no. 2, pp. 241–253, 1984.
- [20] A. M. Smith *et al.*, "Whole brain quantitative CBF, CBV, and MTT measurements using MRI bolus tracking: Implementation and application to data acquired from hyperacute stroke patients," *J Magn Reson Imaging*, vol. 12, no. 3, pp. 400–410, 2000.
- [21] M. I. Townsley, "Structure and composition of pulmonary arteries, capillaries, and veins," *Compr Physiol*, 2012.
- [22] R. Rosencranz and S. A. Bogen, "Clinical laboratory measurement of serum, plasma, and blood viscosity," *Am J Clin Pathol*, vol. 125 Suppl, pp. 78–86, Jun 2006.
- [23] S. Mori, B. Crain, and P. C. van Zijl, "3D brain fiber reconstruction from diffusion MRI," in *Proceedings of International Conference on Functional Mapping of the Human Brain*, 1998.
- [24] J. E. Aarnes, T. Gimse, and K.-A. Lie, *An introduction to the numerics of flow in porous media using Matlab*. Springer Verlag, 2007.
- [25] S. Patankar, *Numerical Heat Transfer and Fluid Flow*, 1st ed. Hemishpere Publishing Corporation, 1980.
- [26] M. Mokin, C. C. Ciambella, M. Masud *et al.*, "Whole-brain computed tomographic perfusion imaging in acute cerebral venous sinus thrombosis," *Interv Neurol*, vol. 4, no. 3-4, pp. 104–112, 2016.
- [27] F. Man, J. T. Patrie, W. Xin *et al.*, "Delay-sensitive and delay-insensitive deconvolution perfusion-CT: similar ischemic core and penumbra volumes if appropriate threshold selected for each," *Neuroradiology*, vol. 57, no. 6, pp. 573–581, 2015.
- [28] P. Kickingereder, A. Radbruch, S. Burth *et al.*, "MR perfusion-derived hemodynamic parametric response mapping of Bevacizumab efficacy in recurrent glioblastoma," *Radiology*, p. 151172, 2015.